The Origin of Differences in the Physical Properties of the Equilibrium Forms of Cytochrome b_5 Revealed through High-Resolution NMR Structures and Backbone Dynamic Analyses[†,‡]

Bindi Dangi,[§] Siddhartha Sarma,[§,||] Chunhua Yan,[§,⊥] Debra L. Banville,[#] and R. D. Guiles*[,§,▽]

Department of Pharmaceutical Sciences, School of Pharmacy, University of Maryland, 20 North Pine Street, Baltimore, Maryland, The Medical Biotechnology Center, an institute of the Maryland Biotechnology Institutes, 725 W Lombard Street, Baltimore, Maryland, and Zeneca Pharmaceuticals, Lead Drug Discovery Group, 1800 Concord Pike, Wilmington, Delaware

Received January 26, 1998; Revised Manuscript Received April 16, 1998

ABSTRACT: On the basis of a comparison of high-resolution solution structures calculated for both equilibrium forms of rat ferrocytochrome b_5, differences in reduction potential and thermodyanmic stability have been characterized in terms of significant structural and dynamic differences between the two forms. The dominant difference between A and B conformations has long been known to be due to a 180° rotation of the heme in the binding pocket about an axis defined by the α- and γ-meso carbons, however, the B form has not been structurally characterized until now. The most significant differences observed between the two forms were the presence of a hydrogen bond between the 7-propionate and the S64 amide in the A form but not the B form and surprisingly a displacement of the heme out of the binding pocket by 0.9 Å in the B form relative to the A form. The magnitude of other factors which could contribute to the known difference in reduction potentials in the bovine protein [Walker, F. A., Emrick, D., Rivera, J. E., Hanquet, B. J., and Buttlaire, D. H. (1988) *J. Am. Chem. Soc. 110,* 6234-6240], such as differences in the orientation of the axial imidazoles and differences in hydrogen bond strength to the imidazoles, have been evaluated. The dominant effector of the reduction potential would appear to be the lack of the hydrogen bond to the S64 amide in the B form which frees up the propionate to charge stabilize the iron in the oxidized state and thus lower the reduction potential of the B form. The structure we report for the A form, based on heteronuclear NMR restraints, involving a total of 1288 restraints strongly resembles both the X-ray crystal structure of the bovine protein and a recently reported structure for the A form of the rat protein based on homonuclear data alone [Banci, L., Bertini, I., Ferroni, F., and Rosato, A. (1997) *Eur. J. Biochem. 249*, 270−279]. The rmsd for the backbone atoms of the A form is 0.54 Å (0.92 Å for all non-hydrogens). The rmsd for the backbone of the B form is 0.51 Å (0.90 Å for all non-hydrogen atoms). An analysis of backbone dynamics based on a model-free analysis of ^{15}N relaxation data, which incorporated axially symmetric diffusion tensor modeling of the cytochrome, indicates that the protein is more rigid in the reduced state relative to the oxidized state, based on a comparison with order parameters reported for the bovine protein in the oxidized state [Kelly, G. P., Muskett, F. W., and Whitford, D. (1997) *Eur. J. Biochem. 245*, 349-354].

Cytochrome b_5 is a b-type cytochrome which unlike other cytochromes plays an essential role in a number of important physiological processes (*1*). In the liver, cytochrome b_5 exists in a membrane-bound form where it serves as an alternate donor to P450 in the metabolism of certain xenobiotics. The membrane-bound forms are also involved in fatty acid desaturation and in cholesterol and testosterone biosynthesis. The membrane-bound form is anchored to the endoplasmic reticulum via a hydrophobic helix. Cytochrome b_5 also exists as a 12 kDa soluble heme-binding domain lacking the hydrophobic helix in erythrocytes where it serves as the terminal electron donor in the reduction of methemoglobin. The soluble heme-binding domain of the protein has been studied extensively crystallographically (*2, 3*) and by NMR[1] solution methods (*4*−*14*).

Cytochrome b_5 has been the subject of numerous studies in recent years for four principle reasons: in complex with its numerous electron-transfer partners as a model system for long-range biological electron transfer (*15*−*18*), to understand protein factors which dictate a marked orientational heterogeneity in the binding of the heme (*12, 19, 20*),

[†] Generous support by the National Institutes of Health (Grant DK 46510) is gratefully acknowledged. Support from the NIH (S10RR10441) for the purchase of a 600 MHz NMR instrument housed in the UMAB NMR facility is also gratefully acknowledged.

[‡] The PDB access codes for the solution structure of rat ferrocytochrome b_5 described here are 1b5a for the A conformation and 1b5b for the B conformation.

[§] University of Maryland.

[||] Current address: Macromolecular NMR Section; ABL-BRP NCI-FCRDC, Frederick, MD.

[⊥] Current address: Genelogic, Columbia, MD.

[#] Zeneca Pharmaceuticals.

[▽] The Medical Biotechnology Center.

S0006-2960(98)00196-2 CCC: $15.00
Published on Web 05/22/1998

as a model system for the study of protein dynamics (*21*), and as a model system for the study of protein interactions with the heme that controls electrochemical properties (*22*−*24*). The structural and dynamic properties of both equilibrium forms of cytochrome b_5 elucidated in this study provide insights into each of these major areas of interest.

The origin of the orientational heterogeneity in the binding of the heme has long been known to be due primarily to a 180° flip about the α,γ-meso carbon axis of the heme in the binding pocket (*5*, *25*). All structural studies to date have focused on the dominant equilibrium form present in solution referred to as the A form. In this report, we describe the differences between the two equilibrium forms based on high-resolution solution structures of both forms in the rat protein where they exist in nearly equal abundance.

EXPERIMENTAL PROCEDURES

NMR Samples. Doubly enriched ^{15}N, ^{13}C samples of cytochrome b_5 were obtained using an *Escherichia. coli* expression system as described previously (*26*). Samples for NMR were prepared in 100 mM phosphate buffer, 10% D_2O and 0.5 mM TSP, pH 7.0. The sample was reduced by purging with nitrogen prior to addition of sodium dithionite. A reducing atmosphere was maintained by sealing the NMR tube under reduced nitrogen pressure with a gas-oxygen torch.

NMR Data Acquisition. All spectra except the HNCO were acquired on a 600 MHz Bruker instrument at 40 °C. The HNCO was acquired on a 500 MHz Varian Unity Plus NMR instrument. The 2D homonuclear NOESY spectra (160 and 200 ms mixing times) were obtained with spectral widths of 8733 Hz in both dimensions. Heteronuclear 3D ^{15}N NOESY-HMQC was acquired with a mixing time of 150 ms. Spectral widths of 3846 Hz in F3 (^{1}H), 1900 Hz in F2 (^{15}N), and 8002 Hz in F1 (^{1}H) were used with 256 real t_1, 64 real t_2, and 1024 complex data points in F1, F2, and F3, respectively. The HNHA (*27*) was acquired with a spectral width of 9765 in F3 (^{1}H), 8333 Hz F2 (^{1}H), and 5000 in F1 (^{15}N) with 2048 × 160 × 100 (complex) data points. The HCCH-TOCSY (*28*) was collected with a spectral width of 8389 Hz in the directly detected ^{1}H dimension, 8401 Hz in the indirectly detected ^{1}H (F2), and 6097 Hz in ^{13}C dimension. The data consisted of 1024 × 256 × 96 complex points. The CBCA(CO)NH was collected using a gradient-enhanced version of the pulse program (*29*) with 2048 × 112 × 88 complex points with spectral widths of 9766 Hz in the ^{1}H, 3041 Hz in the ^{15}N, and 7544 Hz in the ^{13}C dimension. The HNCO was acquired with a gradient-enhanced version of the sequence described by Ikura et al. (*30*) with a spectral width of 8003 Hz in F3 (^{1}H), 2112 Hz in F2 (^{13}C′), and 2200 Hz in F1 (^{15}N). The HNCO was sensitivity enhanced in the ^{15}N dimension, and the acquired data contained 1024 × 100 × 80 complex points. The HCACO was acquired using a gradient-enhanced version of the sequence described by Ikura et al. (*30*) with a spectral width of 8389 Hz in F3 (^{1}H), 5000 Hz in F2 (^{13}C$_\alpha$), and 2500 Hz in F1 (^{13}C′). The HCACO was collected as a constant time experiment and sensitivity enhanced in ^{13}Cα with a digitization of 1024 × 128 × 128. The DQF-COSY was collected with 4096 × 1024 complex points with spectral widths of 8992 in both dimensions. Deuterium-exchange experiments were carried out by dissolving the protein in D_2O and recording HSQC spectra (*31*) at regular intervals (e.g. 10 min, 30 min, 1 h, 2 h, 4 h, 8 h, 16 h, and 32 h). The spectra used for analysis of relaxation parameters consisted of gradient-enhanced, inverse detected 2D HSQC spectra (*32*) recorded with 2048 × 256 complex data points and spectral widths of 8992 Hz in ^{1}H and 2500.01 Hz in the ^{15}N dimension. The relaxation delays used for T_1 inversion recovery were 10, 90, 200, 340, 480, 680, 970, and 1300 ms. The relaxation delays used for the T_2 experiments were 8.1, 16.3, 32.6, 48.9, 65.2, 81.4, 105.9, and 138.4 ms. The heteronuclear NOE (*32*) spectra were acquired in an interleaved manner with a 3 s NOE build-up period for the NOE component of the experiment. Proton chemical shifts were determined relative to an internal TSP (trimethylsilylproprionic acid) reference. Carbon-13 and nitrogen-15 chemical shifts were referenced as described by Wishart et al. (*33*).

NMR Data Processing. All NMR data were processed on Silicon Graphics workstations running Irix 5.3. The 2D NOESY and the 3D NOESY-HMQC were processed using Felix version 2.3 (Biosym Software) as described preivously (*34*). All other data were processed using nmrPipe software (*35*). The HNHA was processed with a cosine bell window function in all three dimensions. The HCCH-TOCSY was also processed in a similar way with a cosine bell window function in all three dimensions. The time-domain data was zero filled in all three dimensions. In addition, the indirectly detected dimensions were extended using linear prediction to give a final matrix size of 1024 × 1024 × 512 (^{1}H,^{1}H,^{13}C). The CBCA(CO)NH spectrum was zero filled to give a final matrix of 2048 × 256 × 256 points. The DQFCOSY was processed with a cosine bell function in both dimensions and zero filled to give a final matrix size of 4096 × 1024 data points. The HSQC spectra used for the relaxation analysis were processed with zero filling in both dimensions and linear prediction in the sensitivity-enhanced dimension to give a final matrix size of 2048 × 512 real points.

Structure Calculations. Structure calculations were performed using DIANA version 2.1 (*36*). FELIX 95.0 was used for database management of the NOE cross-peaks in the 2D NOESY and the 3D NOESY-HMQC. The 3D ^{1}H, ^{15}N, and ^{13}C NOESY was used only to determine if a particular NOE cross-peak contained multiple contributors. The program CALIBA was used for calibration of NOE intensities. Corrections to the cross-peak intensities were

[1] Abbreviations: NMR, nuclear magnetic resonance; TSP, sodium (trimethylsilyl)−propionate; NOE, nuclear Overhauser effect; DQF-COSY, 2D double quantum filtered correlated spectroscopy; TOCSY, 2D total correlation spectroscopy; NOESY, 2D nuclear Overhauser enhancement and exchange spectroscopy; HMQC, 2D heteronuclear multiple quantum correlation spectroscopy; HSQC, 2D single quantum heteronuclear correlation spectroscopy; HCCH TOCSY; 3D double resonance experiment which correlates all protons of a given spin system with the carbons of that spin system; CBCACONH; 3D triple resonance experiment which correlates β-carbon, α-carbon, amide nitrogen, and amide proton resonances; HNCO; 3D triple resonance experiment which correlates amide proton, amide nitrogen and carbonyl carbon resonances; HCACO; 3D double resonance experiment which correlates α-proton, α-carbon and carbonyl carbon resonances; HNHA; 3D double resonance experiment for quantitative J-correlation; NOESY-HMQC; 3D double resonance experiment which correlates dipolar coupled protons to the heteronuclear correlations of the amide spin systems; t_1, evolution time; t_2, evolution time (3D experiments) or data acquisition time (2D experiments); t_3, data acquisition time (3D experiments).

applied to account for the presence of the two equilibrium conformations. The HNHA was used to generate angular constraints for the range of ϕ. This was based on the ratio of the cross-peak to diagonal peak intensity for a given Hα and HN pair. This ratio was used to calculate the J_{HNHA} which in turn was used to calculate ϕ from the Karplus equation (*27*). The DQF-COSY was used in combination with intra and interresidue NOE intensities to assign prochiral protons where possible (*37*). Within the DIANA suite of programs, stereospecific assignments are made in an automated manner using the supporting programs HABAS and GLOMSA. The CBCA(CO)NH and HCCH-TOCSY spectra were used to obtain aliphatic ^{13}C assignments. The C_α assignemts were subjected to a Wishart−Sykes analysis for a preliminary prediction of possible secondary structure elements. Deuterium-exchange rates were used to judge the existence of possible hydrogen bonds. Finally, the NOE distance restraints, the ϕ angle restraints, and the hydrogen bond restraints were used as input for structure calculations. A complete listing of restraints is contained in supplementary Table S-2. Complete REDAC runs were carried out for both the A and the B conformations generating 150 structures during each run. The REDAC runs were performed iteratively until the target functions converged to a minimum value (*36*). The final structures showed no restraint violations and their quality was assessed with the program PROCHECK-NMR (*38*).

Analysis of Relaxation Parameters. The HSQC spectra were analyzed using nmrPipe software (*35*). The peak heights were analyzed using nmrPipe assuming a Gaussian line shape. The relaxation rate constants were then determined by a nonlinear least-squares fit of the experimental peak heights to two parameter single exponential functions. Experimental uncertainties in the measurement of relaxation times were determined from the measurement of replicates of several time points. Errors in the T_1 and T_2 values were estimated by the Monte Carlo type procedures which involve randomly adding or subtracting a number corresponding to the root-mean-square spectral noise from the measured intensities (*39*). The heteronuclear NOE was calculated as the ratio of the peak heights with and without proton saturation. A correction factor was applied to compensate for the incomplete recovery of magnetization during the relaxation delay as described by Grzesiek and Bax (*40*).

Model free analysis of the R_1, R_2, and NOE values was performed using the software ModelFree version 3.1 (*39*). Isotropic and anisotropic models were considered for evaluating the relaxation data. The data were first evaluated assuming an isotropic model using the model-free formalism of Lipari and Szabo (*41, 42*). In this approach, the relaxation parameters are related to the spectral density function as described by Abragam (*43*).

The spectral density function is then modeled as a sum of Lorentzian terms in which the parameters used for describing the dynamic motions of the protein are a generalized order parameter, S^2, correlation times for fast internal motion and global reorientation, τ_e, τ_m, and chemical exchange, R_{ex}. Further S^2 can be considered on a slow time scale (S_s^2) or on a fast one (S_f^2) (*39*). Five models were considered for fitting the experimental data: (1) S^2, (2) S^2, τ_e, (3) S^2, R_{ex}, (4) S^2, τ_e, R_{ex}, and (5) S_f^2, S^2, and τ_e. The selection of a model for a particular residue was based on statistical criteria as previsouly described (*39*). This analysis yielded fits to 67% of the total number of residues examined. A total of 91 residues were examined. Criteria for rejection of peaks for further consideration was based on NOE values (e.g., less than 0.6), overlap of heteronuclear correlation peaks or statistically significant differences in T_1 and T_2 from mean values for the protein which are indicative of slow exchange processes (*44*).

The inability to fit a significant fraction of ther remaining amide vector motions was presumed to be due to the marked physical asymmetry of cytochrome b_5. The programs pdbinertia_1.0 and quadric_1.0 were used to judge the anisotropy of the system. Different diffusional models were examined using the program R_2R_1_1.1. The results showed that an anisotropic model would be the best descriptor for the case of the cytochrome b_5 system. The model-free analysis was carried out again with an individual correlation time for each residue which is expected for a system that exhibits anisotropic diffusion model. The individual correlation times to be used for each residue were calculated by using the program R_2R_1_1.1, which uses the R_2 by R_1 ratios for each residue to determine an estimate of the global correlation time for a particular amide vector (*27*). The individual τ_m values can also be obtained by optimizing the τ_m for each residue by performing a grid search methodology in the model-free program. The results for the τ_m values in the two cases were very similar. The final model-free analyses showed that the difference in the S^2 values for the isotropic and anisotropic models were not significantly different, although an additional 19% of the total number of residues examined was fitted using the anisotropic model. In the final analysis, 76 amide vectors were satisfactorily modeled based on statistical criteria. A statistically significant improvement in fit quality was found with an axially symmetric diffusion tensor model for the global molecular motion of cytochrome b_5.

RESULTS

Sequence Specific and Conformation Specific Assignments. Complete unambiguous assignment of ^{13}C, ^{15}N, and ^1H resonances were based on a set of double and triple resonance experiments. A complete listing of ^1H, ^{15}N, and ^{13}C resonance assignments is contained in Supporting Information Table S-1. Although the vast majority of our ^{15}N and ^1H resonance assignments (*6*) were confirmed, as indicated in Figure 1, there were some startling exceptions. Through bond linkage to the previously assigned α-protons of G41 is shown in Figure 2 in a 2D section of the HNHA. The α-protons had been previsously assigned based on ring-current calculations and the presence of a peak in the DQFCOSY, which was characteristic of a glycine α,α′ cross-peak at 0.37 and 3.37 ppm (*6*). Unambiguous assignment of the amide proton of G41 to a resonance at 1.04 ppm for the A form (1.10 ppm for the B form) was established by connectivies observed in the CBCACONH spectrum shown in Figure 3. This is the highest field amide proton resonance assigned to date. Totally unambiguous side-chain assignments confirming this assignment path and for the majority of the residues in the protein were obtained from highly resolved complete proton ladders observed in HCCH TOCSY spectra (See Figure 4). On the basis of these methods, all protein resonances of the four helix bundle binding the heme

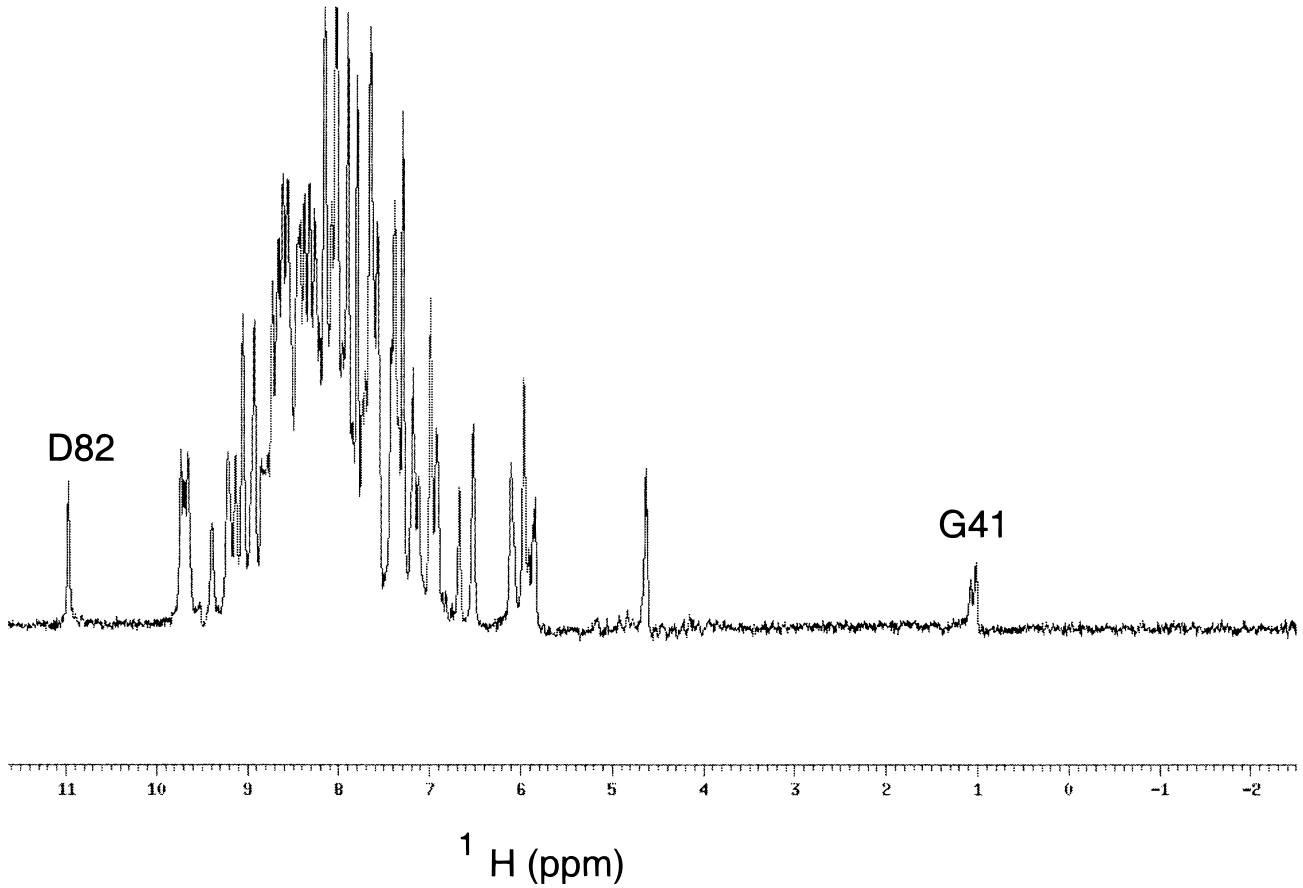

FIGURE 1: An ^{15}N edited proton 1D spectrum of ferrocytochrome b_5 obtained from the first slice of an HSQC specturm. The amide proton of D82 at a proton chemical shift of 10.98 and G41A at a proton chemical shift of 1.04 ppm are indicated.

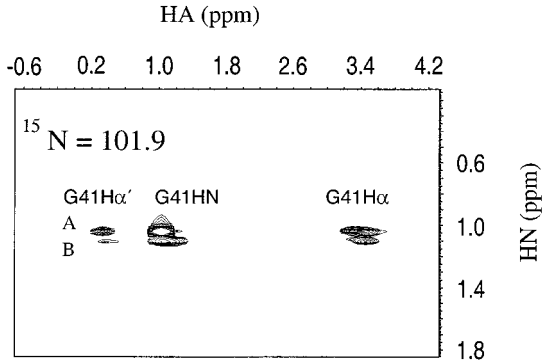

FIGURE 2: A 2-dimensional section from an HNHA spectrum corresponding to an ^{15}N chemical shift of 101.9. This ^{15}N chemical shift was identified in the ^{15}N-^{1}H HSQC spectrum. This plane shows correlations between the two α protons and the amide proton of G41A and B.

group were assigned. Once we had this complete set of assignments, assignment of the only remaining protons unassigned on the heme cofactor became unambiguous. NOESY connectivities between the methylene protons of the propionates and adjacent protons on the heme and to surrounding residues enabled assignment of these protons. Chemical shift values for the α-methylene protons were observed at 4.12 ppm, and the chemical shift of the β-methylene protons were observed at 3.10 (β) and 2.93 ppm (β'). The chemical shift values for these sets of protons were virtually degenerate for both propionates; however, the β' resonance is significantly different in A and B forms. Chemical shifts of the propionate protons are similar to those recently reported for a monomeric diamagnetic hemoglobin (*45*) and are consistent with averages of values reported for heme proteins recently compiled by Banci et al. (*46*).

Structure Calculations. Structure calculations were performed for the soluble heme-binding domain of cytochrome b_5. Residues 1−94 were considered. Residues 1−3 and residues 87−94 belong to unstructured domains of the protein (*3*). Structure calculations were carried out using 1218 distance restraints for the A conformation and 1152 distance restraints for the B conformation. This amounts to approximately 15 restraints per assigned, structured residue, not including the dihedral angle described below. The type of restraints classified as intraresidue, medium range, and long range are outlined in Figure 5. A chemical shift analysis of the Cα ^{13}C chemical shifts was performed using the Wishart−Sykes method (*47*). The results are shown in Figure 6.

Restraints for 70 ϕ angles were calculated from the HNHA. Deuterium-exchange rates were calculated for the amide protons of the A and B conformers. These rates were assigned arbitrarily into three categories; fast exchanging (less than 10 min), intermediate exchanging (10 min to 10 h), and slow exchanging (greater than 10 h) results are shown in Figure 7. The amide protons which were in the slow-exchange category were considered for involvement in hydrogen bonds by comparison with the consistent hydrogen bonds as reported by the structure calculation program. A total of 70 such hydrogen bonds were used to generate distance constraints between the amide proton and a hydrogen bond acceptor with an upper bound of 2.4 Å and a lower

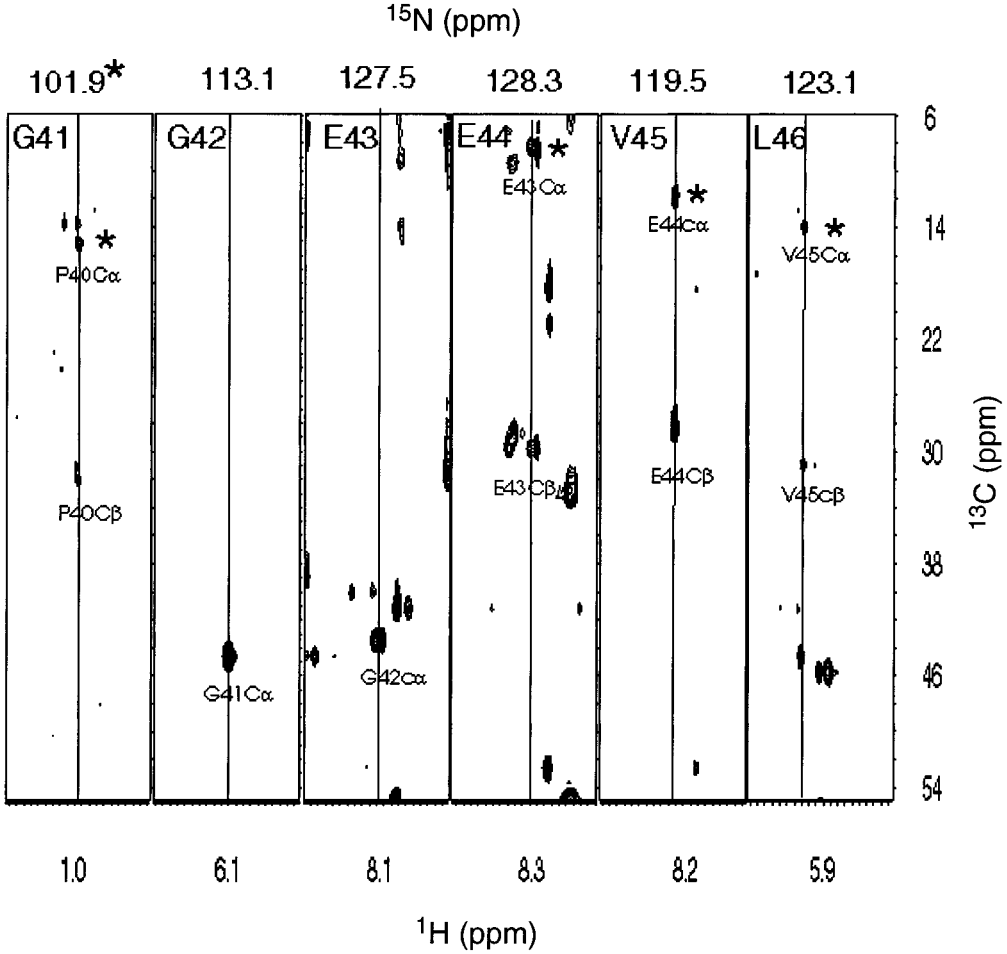

FIGURE 3: 2D sections of a CBCA(CO)NH spectrum corresponding to residues G41 to L46. Each plane corresponds to the amide ^{15}N chemical shift of the residue indicated in the top left corner and shows correlations to the C_α and C_β carbon nuclei of the $i-1$ residue. (*) Note that for a number of residues shown: the $^{13}C_\alpha$ resonance is folded.

bound of 1.5 Å (*48*). The final structure calculations showed no restraint violations greater than 0.4 Å and yielded an RMSD for backbone atoms of 0.5 Å for both the conformations. An overlay of the top 20 structures is shown in Figure 8.

An analysis of the ensemble of the top 20 structures for each conformation was performed using PROCHECK-NMR. The Ramachandran distribution is shown for the A and the B conformers in Figure 9. The distribution of the ϕ and ψ angles for both the conformers is indicative of the quality of structures calculated. Both the A and the B conformer show more than 74% of the residues in the most favorable region, indicating structures equivalent to a 2 Å resolution X-ray structure. A Ramachandran plot for the average structure indicated that 80% of the residues were in the core region and 20% were in the allowed regions. None of the residues were seen to lie in the disallowed regions for either the A or the B form of the protein.

Analysis of Residues in the Heme Binding Region. Unique restraints for the A and the B form were observable from the heme to the surrounding residues. As we have previously indicated, these NOESY connectivities are the primary basis of conformation specific assignment (*7*). The heteronuclear methods added confidence to our previous assignments by providing unambiguous through-bond linkages establishing all resonances associated with a given spin system. The number of long-range restraints from the heme group to the protein for the A and the B conformers were 43 and 30, respectively. Unique restraints for the A and the B conformers were also identifiable for almost all residues in the heme binding region (W22−Y74). A planar heme geometry was used in the final structures reported here. Structures calculated using the nonplanar heme geometry reported by Mathews (*3*) for the A form of the bovine protein did not show any significant differences in structure quality or structural features from the geometry calculated using a planar heme. The ability to discern distortions from a planar heme geometry is clearly a significant advantage of X-ray crystallographic methods.

A superior number of long-range restraints for the residues in the heme-binding region enabled us to characterize the geometry of residues more precisely than has earlier been reported (*11*). This has been possible through the use of heteronuclear NMR techniques described in greater detail below. The geometry of the axial ligands, His39 and His63, was extremely well-defined through over 75 restraints for both the A and the B conformers. Almost 40% of these restraints were long range, and this enabled determination of the relative orientation of the axial ligands with respect to the surrounding residues and the heme moiety. An overlay of the X-ray structure (3*b*5c) with the A and B conformers did not indicate any significant differences in the backbone geometry for either the A or the B form of the protein. A comparison of the A and B conformers revealed that the

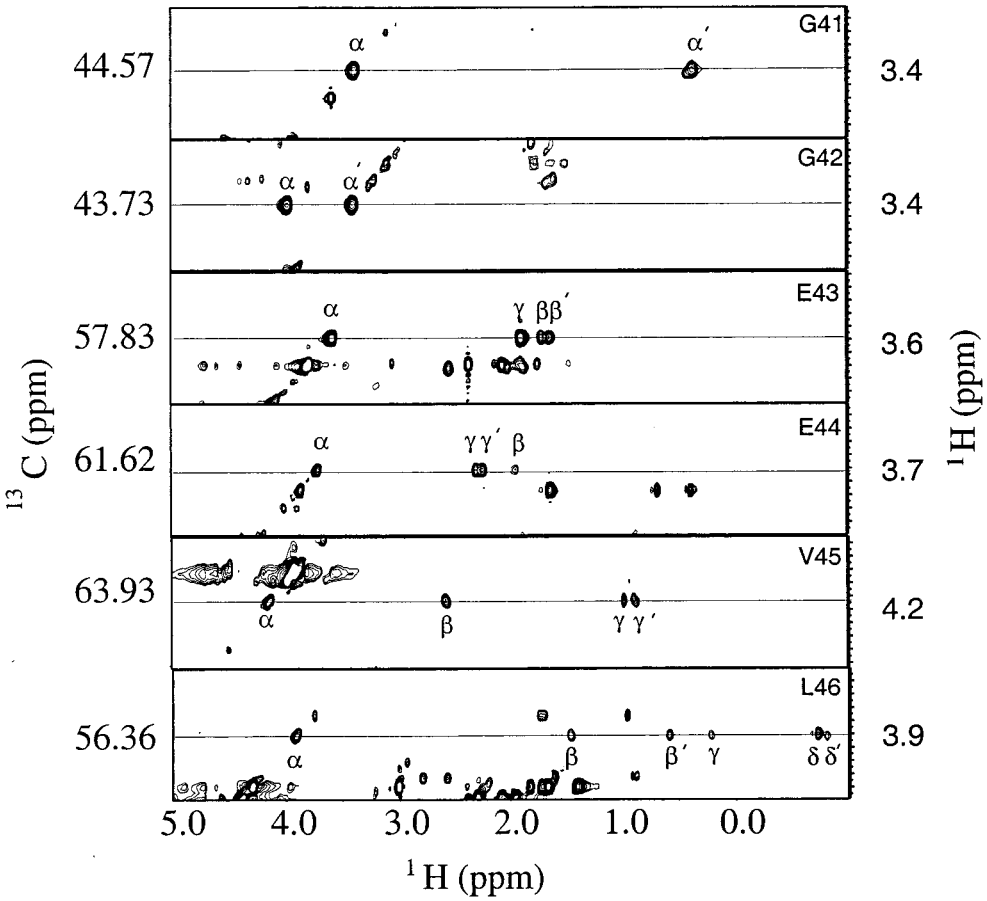

FIGURE 4: 2D sections of the HCCH-TOCSY corrresponding to the ^{13}C chemical shift of the C_α nucleus as indicated by the CBCA(CO)NH spectrum confirming the $i - 1$ correlation. Each 2D section shows the complete proton ladder at the C_α proton chemical shift for the residue indicated in the top right corner of each 2D section.

backbone geometry was largely the same for both and that the rmsd for the backbone between the two conformers was 0.8 Å. Small differences are evident between the two conformations in the region of helix 3, as can be seen in the overlay of the average structures shown in Figure 11.

The primary focus of this study was to examine differences between the two conformers, which in turn would provide insight into factors controling heme electroreactivity and the differing thermodynamic stability of the two conformers. Some of the surprising differences observed between the two conformers are outlined below. Figure 11A contains an overlay of the average structure for both A and B conformors, highlighting differences between them. A 5−10° in plane rotation in addition to the ring flip has previously been suggested (*6, 19*). This conclusion was based on a limited set of NOEs from the surrounding residues to the heme prosthetic group. Although within the limits of uncertainty observed, this 5−10° in-plane rotation is indeed possible, an additional unexpected feature was the observed heme ring displacement from the heme cavity toward the solvent in the B form by nearly an angstrom. The position of the heme ring in the two conformers is very well-defined and the standard deviation of the Fe center found in the rms overlay of backbone structures in both the conformations is 0.2 Å. The average inplane displacement of the heme iron between the two structures is 0.9 Å. Thus, our statistical confidence in this displacement, given two sets of 20 structures, is greater than 95% based on a Student's *t*-analysis of the difference between the two means (*49*). Figure 11B illustrates this shift through an overlay of the hemes taken from the rms overlay of the backbone structures shown in Figure 11A. Some other differences in the B conformation were the possibility of angular displacement of His 39 from the normal to heme plane similar to the observation in the A67V mutant (*34*). This effect could play an important role in modulating the electrochemical properties of the heme center; however, the magnitude of the imidazole reorientation is significantly smaller between the A and B conformers than that we observed between the wild-type and the A67V mutant.

Another very important observation in the B form is the absence of a hydrogen bond between the main-chain amide proton of Ser 64B and the heme propionate. This hydrogen bond was, however, seen in the A form of the protein. This hydrogen bond has not been reported in the recently published solution structure of the major form of rat cytochrome b_5 (*11*). The assignment of this hydrogen bond which is observed in the bovine crystal structure is based on three lines of evidence. Structure calculations performed by Diana 2.1 reported the formation of a consistent hydrogen bond between the heme propionate and the amide proton of S64A based on a set of NOEs to the β-CH_2 protons of the heme propionate-7 (e.g., NOEs observed between the β-CH_2 of the 7-propionate and the 8-methyl of the heme and the β-methyl of A67). The existence of the hydrogen bond is also indicated by a more than 10-fold difference in hydrogen-exchange rates between S64A and S64B. Finally, the dynamic analysis indicates a significantly more restricted amide bond vector in S64A relative to S64B. This difference

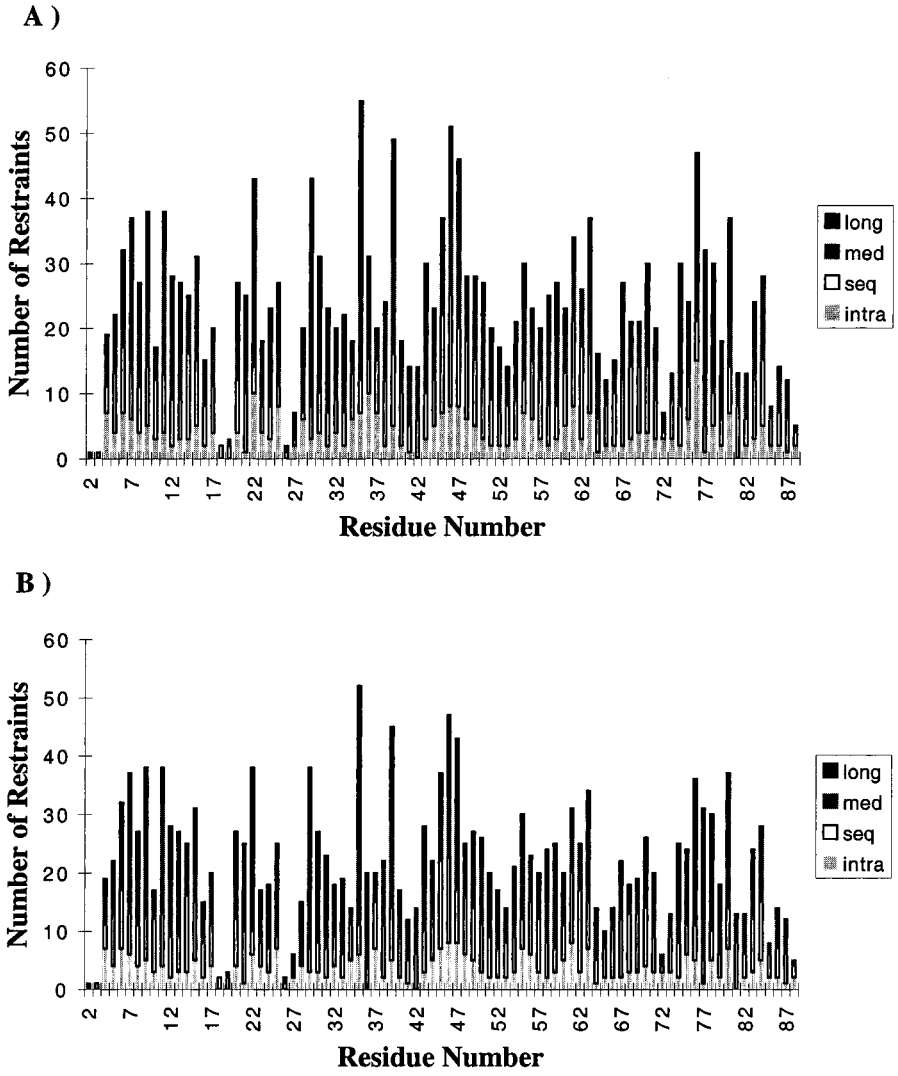

FIGURE 5: Plots showing the restraint distribution for the two conformations. (A) Distribution for the A conformer and (B) Distribution for the B conformer. The distribution shows intraresidue restraints (intra), sequential restraints (seq), medium range restraints (med), and long-range restraints (long) corresponding to restraints between residues separated by more than three amino acids. Restraints not shown in the above plot are the 40 long-range restraints observed for the heme prosthetic group in the A conformer and the 30 such restraints for the B conformer.

corresponds to an increased range of angular movement of the S64 amide vector by 4.5° assuming a model of the motion in which the amide vector is free to move about within a conical domain (*41*). Although both the vinyl and propionate group dihedral angles were free to rotate, the final geometry of the heme group showed that the vinyl groups retained the geometry in the crystal structure while the propionate groups were more flexible.

Dynamics of Cytochrome b_5. (1) Deuterium-Exchange Rates and Mobility. An analysis of deuterium-exchange rates was performed for ferrocytochrome b_5 and are represented in Figure 7. Residues which showed deuterium-exchange rates less than 10 min or could not be accurately quantitated due to spectral overlap are not shown in the figure. Most of the residues which showed deuterium-exchange rates faster than 10 min were confined to the N- and C-termini. Other residues which showed fast deuterium-exchange rates were located in α1 and α3, β3, and regions on the surface of the molecule. These regions were seen to be dynamic in the molecular dynamics simulations as well and thus these enhanced exchange rates may correlate with certain breathing modes of the protein (*21*).

(2) Relaxation Rates. T_1, T_2, and heteronuclear NOE values were calculated based on peak heights determined from Gaussian line shape fits to the heteronuclear correlation peaks. Single two parameter exponential fits were used in the determination of T_1 and T_2. Figure 12 contains a plot of the amplitudes of these relaxation parameters plotted as a function of residue number for the A conformer.

The dimensions of cytochrome b_5 determined from the X-ray and solution structure indicate an ellipsoidal shape. The program inertia_1.0, distributed with the Modelfree 3.1 suite of programs, revealed that the relative moments of inertia were 0.6472:0.8794:1.0000. The R_2/R_1 ratio was used to calculate the appropriate τ_m for each residue. These values corroborated the values obtained from the Modelfree program which was used to optimize the τ_m for each residue. These τ_m values were used for performing the quadric diffusion analysis (*50*), the results of which are summarized in Supporting Information Table S-3.

The isotropic results returned a value of $(2.794 \pm 0.002) \times 10^7$ s^{-1} for Diso. The axial results indicated a value of 1.18 for Dpar/Dper (axial ratio), and the anisotropic results gave a value of 1.19 for 2Dzz/(Dxx+Dyy). Finally the

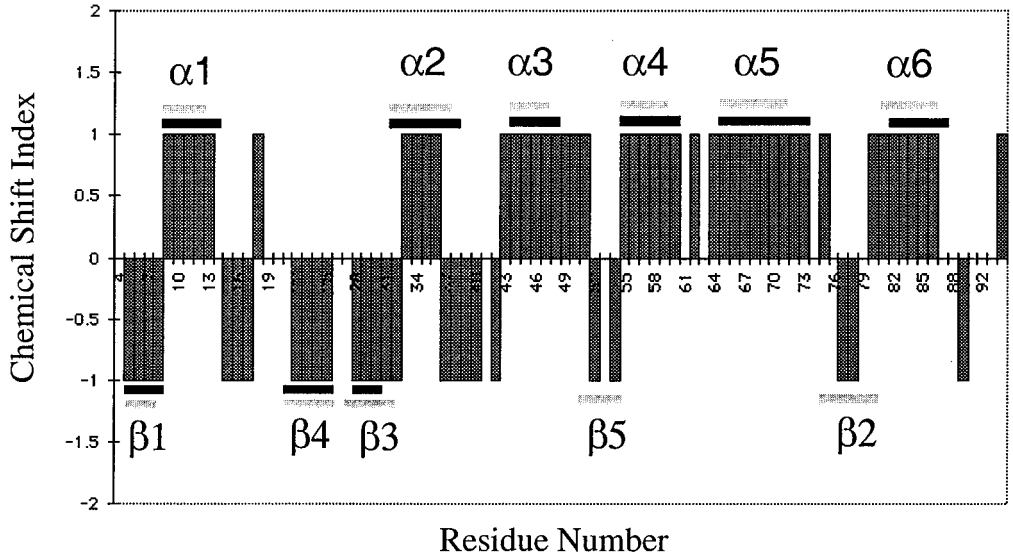

FIGURE 6: A plot of the chemical shift index 1, 0, −1 (*47*) plotted against the residue number. A group of (sequential) three or more vertical bars with a value of −1 indicate the possibillity of a beta sheet while a group of three or more vertical bars (sequential) with a value of +1 indicate the possibility of an α helical structure. The gray horizontal bars indicate the ranges of secondary structural elements as seen in the bovine X-ray crystal structure (*3*) and the black horizontal bars indicate the ranges as seen in the present NMR solution structure. These ranges were determined through an analysis of ϕ and σ angles as described in the text.

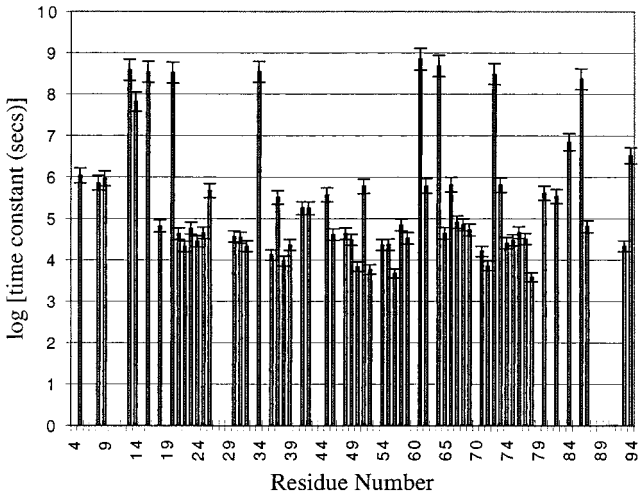

FIGURE 7: A plot of the deuterium exchange time constants as a function of residue number. The log of the time constant (seconds) is plotted because of the enormous range in the deuterium exchange rates for the protein.

model-free version 3.1 was used to obtain S^2 and τ_e values given individual optimized τ_m values for each residue. The choice of the best diffusional model for cytochrome b_5 was based on the improvement in fit quality using an *F*-test comparing critical values at the 95% confidence level (See Table 1). The S^2 values for the various residues are tabulated in Supporting Information Table S-3. The average S^2 value for the system was 0.87 indicating a relatively rigid system. The analysis was carried out for both the A and B conformations. The majority of the residues showed similar behavior in terms of S^2. Table 4 contains a listing of residues which display signficant differences.

DISCUSSION

The Origin of Differences in Electrochemical Properties. Several theories exist regarding protein heme interactions which modulate cytochrome reduction potentials. The effects of axial imidazole orientation (*51*), hydrogen bonding to the axial imidazoles (*52*, *53*) and the effects of charge distributions in the vicinity of the heme (*54*) are currently thought to be the most significant effectors. The magnitude of each of these effects has been evaluated with regard to differences observed between the two equilibrium conformations. As indicated in our previous studies of rat cytochrome b_5, the strengths of hydrogen bonds between the axial imidazoles and main-chain carbonyl atoms are not significantly different in the two conformers as is indicated by the similarity in the chemical shifts of imidazole Nδ1 proton and ^{15}N resonances (*24*). Similarly, based on a comparison of the structures calculated for both the A and B conformations, it would appear that axial imidazole ring reorientation is much smaller than that we have observed in a mutational study which was designed to perturb the ring orientation (*34*). However, the one significant difference, other than the displacement of the heme out of the binding pocket by nearly an angstrom, is the observation of a hydrogen bond between one of the heme propionates and the S64 amide in the A form and not the B form.

On the basis of the X-ray crystal structures of both oxidized and reduced states, Mathews et al. (*3*) proposed that the structures of the oxidized and reduced protein of cytochrome b_5 are virtually identical except for a cation that binds to the propionate group in the reduced protein to neutralize the negative charge. It is believed that when cytochrome b_5 is in the ferric state, the iron atom has a formal charge of +1. This charge is controlled by the conformation of the heme propionates, since it is believed that these groups play an important role in neutralizing this charge. In the bovine protein, S64 plays an important role in orienting one of the heme propionates by forming two hydrogen bonds, one with the main-chain amide and the other with the side-chain hydroxyl group. A number of mutagenic (*23*), chemical modification (*55*), and crystallographic studies (*23*) have revealed that this hydrogen bonding plays an important role in modulating the electrochemical properties of the heme center. A study of the S64A mutant of cytochrome b_5

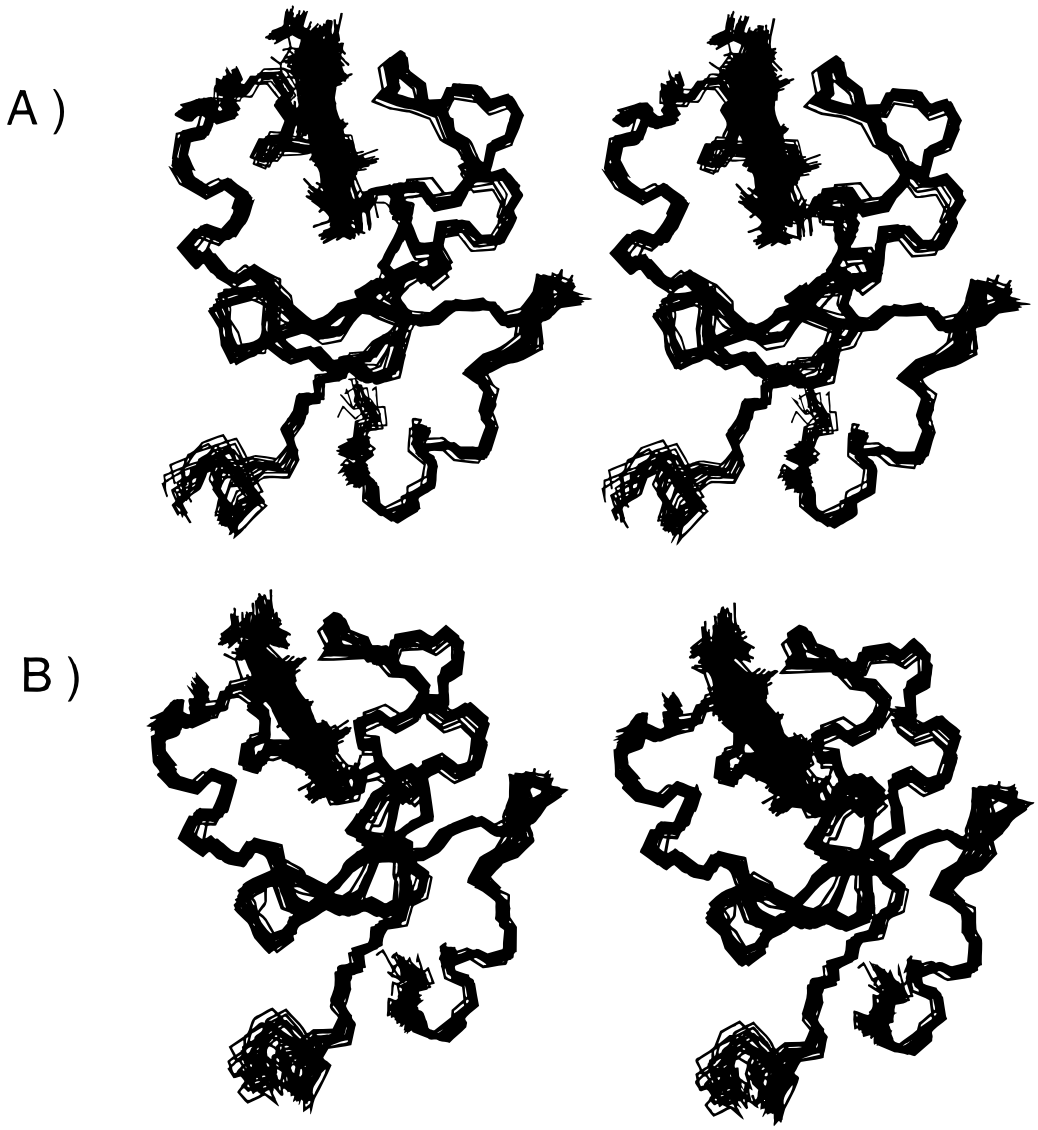

FIGURE 8: A stereoview of the an rms overlay of the top 20 structures with the lowest target function values output by DIANA. (A) A conformation, (B) B conformation.

showed that this alanine mutant had a lower reduction potential. It was believed that this was primarily due to the inability of this mutant to form a hydrogen bond with the heme propionate. This allowed the heme propionate to stabilize the +1 charge at the iron center in the oxidized protein which, in turn, corresponded to a lower reduction potential. We have made a similar observation in comparing the structures of A and B forms of rat cytochrome b_5. Although the A conformer showed the hydrogen bond with the S64HN, the B conformer did not. This was presumably due primarily due to the positional shift of the heme ring in the binding pocket. This observation correlates well with the lower reduction potential of the B conformtation (27 mV lower than that of the A) in that the propionate is more available to stabilize the positive charge of the iron in the oxidized state if it is not tied up with a hydrogen bond to the S64 amide (*23*). Thus, the rat system has proved to be an ideal system where one can correlate structural changes between conformational states to differences in reduction potential through the use of heteronuclear NMR methods.

Differences in the Thermodynamic Stability of the A and B Conformers. A number of studies have also implicated the heme propionates in controlling the ratio of the conformational isomers in myoglobin and cytochrome b_5 (*56*, *57*). This ratio has been correlated to the degree of hydrogen bonding possible and the kinetics of heme dissociation. The existence of a hydrogen bond stabilizes heme binding and improves thermodynamic stability of the conformation, as is indicated by a preference for one equilibrium conformation over the other. Comparisons between species variants have also implicated a cluster of hydrophobic residues in contact with the 2-vinyl group of the heme in the B form which presumably detabilizes the heme binding. It is now clear from the detailed study of the structures of the two conformers that both of these effects are correlated. Steric interactions of the 2-vinyl group of the heme in the B conformation are the principle cause of the heme displacement out of the heme-binding cavity which then prevents the formation of the hydrogen bond between the S64 amide and the heme propionate. Recently, mutagenic studies have implicated residue 74 (residue 74 is a phenylalanine in the bovine protein and a tyrosine in the rat protein) in modulating the equilibrium ratio of conformational states. We believe this role may be mediated by orienting F35 in its interaction with

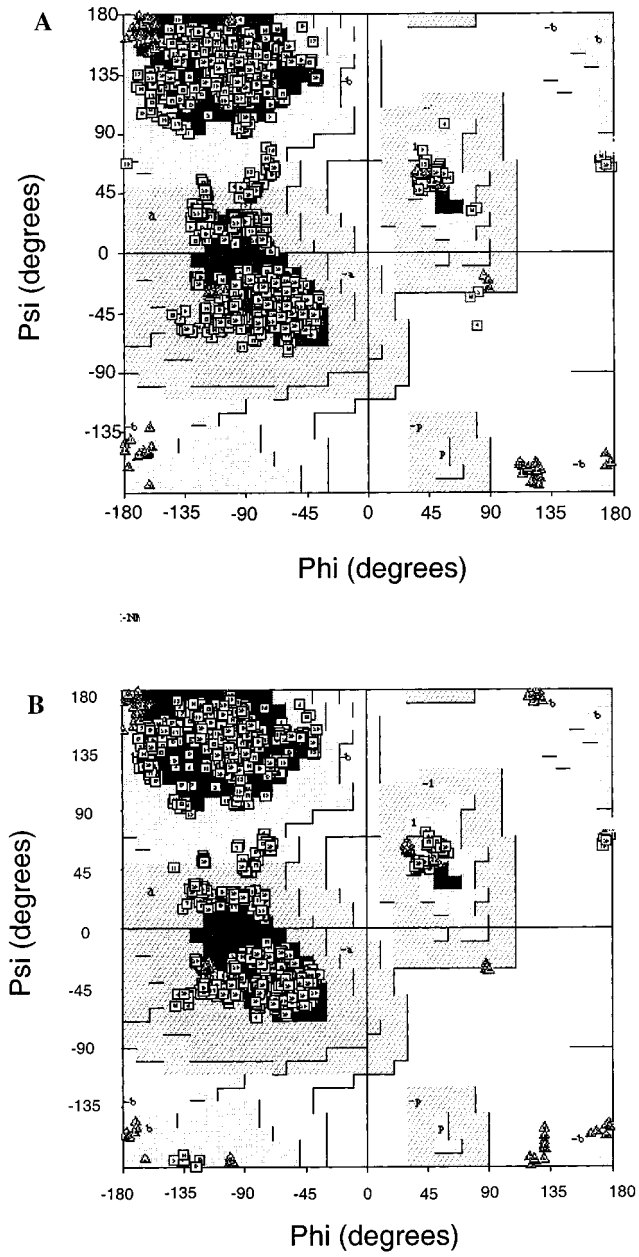

FIGURE 9: (A) The distribution of the phi and psi angles for the top 20 structures as calculated by PROCHECK-NMR. The triangles correspond to glycine or proline residues. The distribution of the backbone dihedral angles for the A conformer were 75.1% in the core, 24.0% in the additional allowed regions, 0.8% in the generously allowed regions. (B) The distribution of the backbone dihedral angles for the conformer were 74.5% in the core, 24.9% in the additional allowed regions, 0.6% in the generously allowed regions. Neither the A nor the B conformer showed any non-glycine or proline residues in the disallowed regions.

the heme. Both F35 and F58 stabilize the heme binding through hydrophobic aromatic overlap with the heme ring system. The 0.9 Å displacement out of the heme pocket reduces this overlap substantially and, hence, presumably reduces the thermodynamic stability of heme binding. It is important to note that in virtually all other species variants of cytochrome b_5 the residue at position 23 is a leucine or an isoleucine (*3*) (in the rat protein it is a valine). As can be seen from Figure 14, residues V23, L25, and L46 form a tight cleft on which the 2-vinyl group in the B form sits. If V23 is replaced with a leucine, this cleft is presumably reduced in volume and the heme would be even further displaced out of the binding pocket further reducing the thermodynamic stability of the B form in these other species variants as is observed.

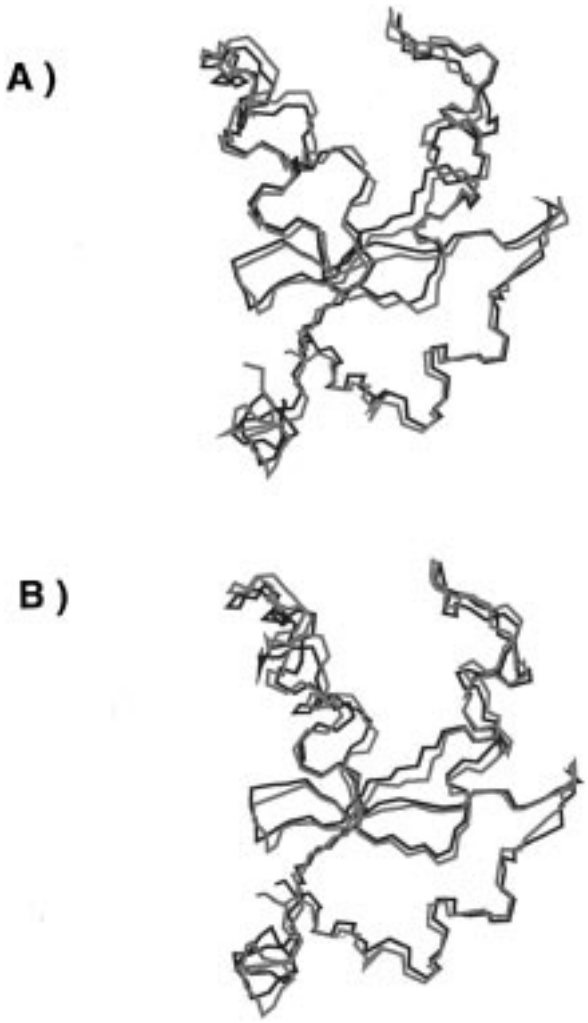

FIGURE 10: (A) An overlay of the average backbone structure of the A conformation (calculated using XPLOR) with the bovine X-ray crystal structure (red) and (B) shows an overlay of the average backbone structure of the B conformation with the X-ray crytal structure (red).

Comparisons with Other Structures. An overlay of the backbone of the X-ray structure and the solution structure is shown in Figure 10. An rmsd of about 1.0 Å was observed between the bovine crystal structure and the rat solution structure for both the conformations (backbone atoms C_α, carbonyl, and amide N). Recently, a large number of groups have investigated differences in the secondary structural elements of the X-ray structure with the solution structures of various species variants. A comparison of the quality of these structural analyses is contained in Table 2. Pairwise rmsd calculations were performed between the solution structures of both the A and B forms reported here and the recently reported structure of the A form reported by Banci et al. (*11*), the bovine X-ray crystal structure, and the solution structure of the oxidized bovine protein (*10*). Other recently reported solution structure analyses have heavily relied on analysis of homonuclear data (^{15}N data was used in the analysis of the oxidized bovine solution structure). Our ability to double label cytochrome b_5 has enabled us to obtain ^{13}C assignments for most of the aliphatic carbons. Tables

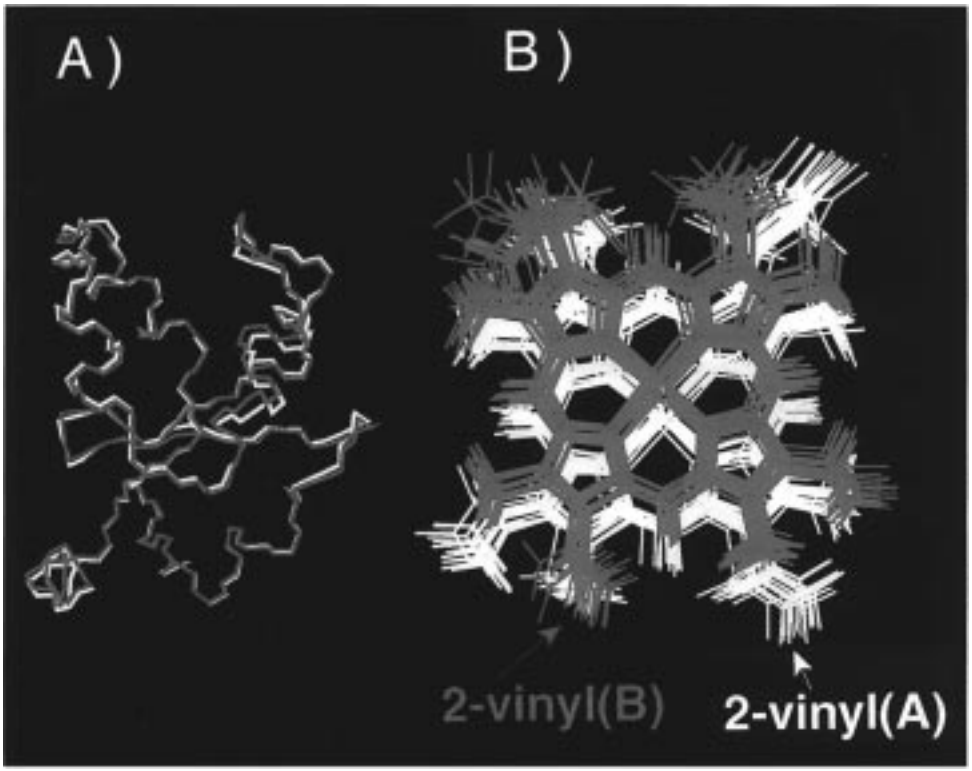

FIGURE 11: (A) An overlay of the average backbone structure of the A conformer (white) with the B conformer (red) backbone structure. (B) An overlay of the heme groups (top 20 structures, with the backbone atoms aligned) of the A (white) and B (red) showing the displacement of the heme in the B conformer out of the binding pocket by 0.9 Å.

for these assignments are available in Supporting Information (see Table S-1). A Wishart−Sykes analysis can be performed for the H_α, C_α, and the CO chemical shifts and has been used extensively as a predictor of secondary structural elements (*47*, *58*). In the case of cytochrome b_5, we were restricted to the use of ^{13}C chemical shifts since proton chemical shifts are strongly influenced by proximity to the heme system. For example, as indicated above, glycine 41A, which has the HN proton closest to heme group, shows a chemical shift at around 1.0 ppm. The H_α protons of this G41 are at 3.37 and 0.37 ppm. The random coil chemical shift for a glycine α-proton is 3.95 ppm and that of the amide proton is 8.39 ppm (*59*). These ring-current shifts preclude the possibility of using H_α chemical shifts for chemical shift refinement. An analysis of the $^{13}C_\alpha$ chemical shifts is shown in Figure 6.

An analysis of the ϕ and ψ angles of the top 20 structures of A and B conformations was also performed. The average ϕ and ψ angles for the ensemble of structures were analyzed in order to evaluate ranges of secondary structural elements. The criteria used was based on ranges used for prediction of secondary structure by Daggett and Levitt (*60*). Most of the secondary structural elements were consistent with those observed in related solution structures. Molecular dynamics simulations performed on cytochrome b_5 have shown that α1, α3, α4, β1, and β4 are the most stable secondary structure elements (*21*). A Wishart−Sykes analysis of the ^{13}C chemical shifts could succcessfully predict the presence of α1, α3 α4, α5, and α6. However, the α2 strand indicated in the crystal structure was found to be irregular. This observation is consistent with previously reported NMR structures (*10*, *11*, *14*). As far as the β-strands were concerned, β1 and β4, which were predicted to be the most stable β-strands by the molecular dynamics simulation, could be unambiguously predicted from the chemical shift analysis. Recent structural studies carried out on the oxidized and reduced forms of the protein were not able to successfully predict the presence of β1. The rest of the secondary structure analysis was largely consistent with previously reported data. The backbone rmsd of the A form of the protein versus the B form was found to be 0.5 A. The secondary structural elements were largely unperturbed in the B form of the protein.

Dynamics of Cytochrome b_5. A number of groups have recently studied dynamics of redox proteins in more than one oxidation state either theoretically (*61*, *62*) or based on deuterium exchange (*63*). Certain proteins are believed to undergo significant structural reorganization when going from one redox state to another (*63*, *64*). The reorganizational energy involved in this process may play an important role in the rate of electron transfer. Recent structural studies on oxidized (*14*) and reduced cytochrome b_5 (*11*) reveal that only minute differences exist between the two states consistent with the X-ray crystallographic characterization of both oxidation states for the bovine protein (*3*). Dynamic studies have also been performed for 55 residues of the major form of the oxidized form of bovine cytochrome b_5, assuming an isotropic model (*4*). Here, we have analyzed 76 of the 94 residues of both equilibrium forms of reduced rat cytochrome b_5. The results indicate that the reduced form of cytochrome b_5 is a more rigid system [e.g., our average squared order parameter is 0.87 while that reported by Kelly et al. (*4*) has an average of 0.8]. We have also completed a careful comparison of the dynamics of both oxidation states of rat cytochrome b_5 examining the effects of the paramag-

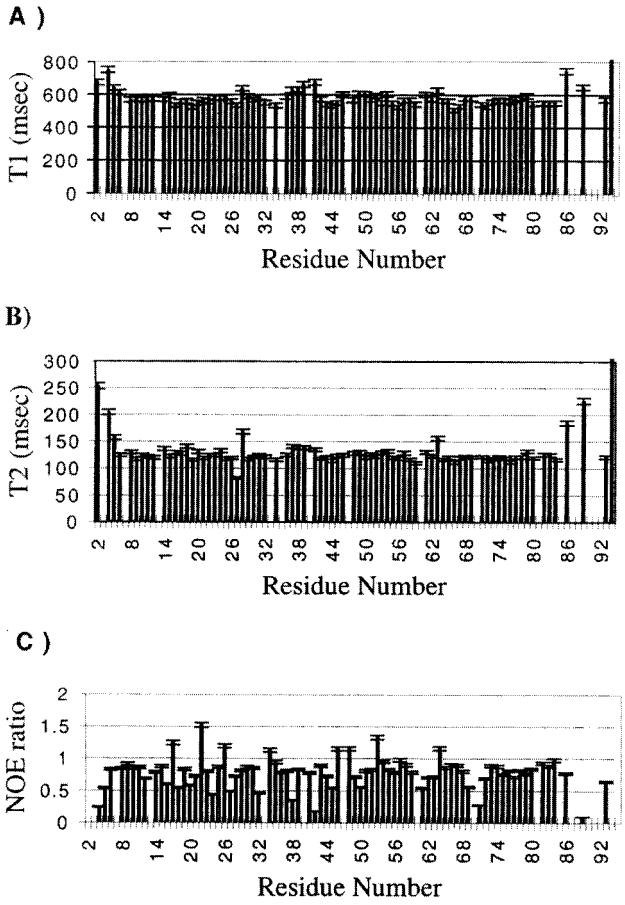

FIGURE 12: (A) T_1 values (ms) plotted against residue number; L94 shows a T_1 value of >800 ms and is off scale in the figure. (B) T_2 values (ms) for each residue; L94 shows a T_2 value >300 ms and is off scale in the figure. (C) Heteronuclear NOE ratios plotted against residue number.

Table 1: Statistics on the Analysis of Diffusional Models for Cytochrome b_5

	$\chi 2$	$\chi 2$ red[a]	F[b]
isotropic	7812.481	114.8894	
axially symmetric	6749.749	103.8423	3.411
anisotropic	6667.296	105.8301	0.384

[a] The reduced χ_2 is normalized to the number of degrees of freedom in the measurement. [b] For 76 measured values and one parameter in the fit versus three parameters in the fit for the axial case, the critical value for the *F*-statistic at a 95% confidence interval is 3.14 (*49*).

netism on the relaxation rates at mulitple fields, and the results will be presented in a subsequent paper (*65*).

Certain differences do exists in the deuterium-exchange rates and the backbone dynamics of the A and the B conformers. The residues showing significant differences in the deuterium-exchange rates and the S^2 values are indicated in Tables 3 and 4, respectively. Perhaps surprisingly, although there are differences in the magnitudes of both the order parameters and deuterium-exchange rates, they do not correlate strongly.

No obvious correlation between regions of high dynamic mobility observed in molecular dynamics simulations of cytochrome b_5 (*21*) have been observed with the order parameters, but many of the reported fluctuations in the structure of cytochrome b_5 were on relatively long time scales and may not be well sampled by the ^{15}N relaxation analyses.

Table 2: RMSD[a] Comparison of the A and B Conformations of Rat Cytochrome b_5 with Related Structures

structure[b]	A conformer	B conformer
top 20 structures	0.54	0.51
1AQA	1.54	1.56
3B5C	0.94	1.01
1WDB	4.29	3.31
1CYO	0.95	1.01
between the two conformers	0.52	0.52

[a] The RMSD comparisons were based on an XPLOR analysis of the top 20 structures for each conformer. The average structure calculated by the program was then used to make comparisons with other reported structures. [b] The 4 digit pdb codes have been used to designate the related structures. 1AQA: reduced rat cytochrome b_5, NMR solution structure (A form) (*11*). 1WDB: oxidized bovine cytochrome b_5, NMR solution structure (A form) (*10*). 3B5C: oxidized structure of bovine cytochrome b_5, 2.0 Å resolution (A form) (*3*). 1CYO: average minimized bovine cytochrome b_5, 1.5 Å resolution (A form) (*66*).

Table 3: Comparison of Deuterium Exchange Time Constants of the A and B Conformations of Cytochrome b_5[a]

residue	ratio of time constants (*A/B*)
34	2488
37	0.529
39	1.537
45	1.610
46	1.596
48	0.513
49	5.532
51	1.397
52	0.136
61	46265
64	10.11
66	2.149
72	1.392
73	1.478
74	1.103

[a] The table shows the ratio of the time constants for deuterium exchange (*A/B*) for residues of ferrocytochrome b_5. The time constants for each residue were obtained by fitting peak heights in ^{15}N-edited HSQC spectra (obtained at intervals of 10 min, 30 min, 1 h, 2 h, 4 h, 8 h, 16 h, and 32 h) to an exponential decay function using Excel. The average error in the determination of these deuterium exchange time constants was 3%. This error was determined by carrying out the experiment in duplicate.

Deuterium-exchange studies are more suited to such long time scale structure fluctuations. Among the helices that form the four helix bundle, helix 3 has the fastest deuterium-exchange rate, consistent with long-time scale and perhaps low-frequency conformational changes predicted by the molecular dynamics analyses. Fluctuations in the position of helix 3 which contains two residues implicated in interprotein recognition could play an important role in cytochrome b_5's ability to interact with several different electron-transfer partners.

ACKNOWLEDGMENT

We are indebted to the Nuclear Magnetic Resonance. Facility at Madison for providing NMR pulse programs for many of the experiments described in this study. Special thanks to Dr. Brian Volkman for assistance with the implementation of many of these sequences. We also thank Dr. Russell J. DiGate for assistance in the reengineering of the synthetic gene construct originally provided by Dr. Steve

Table 4: Comparison of S^2 Parameters for the A and B Confomations of Cytochrome b_5[a]

residue	A conformer	B conformer
25	0.95	0.88
41	0.83	0.88
44	0.79	0.97
46	0.95	0.90
50	0.84	0.88
53	0.93	0.85
55	0.93	0.88
57	0.92	0.88
61	0.83	0.87
63	0.81	0.73
64	0.92	0.86
66	1.00	0.87
71	0.75	0.85
73	1.00	0.89

[a] The S^2 values shown are only for those residues where the values differed by more than 3 standard deviations beyond the uncertainty in the measurements. The average error in the estimation of the S^2 value was 0.009 which was determined by the model-free analysis as described in the text.

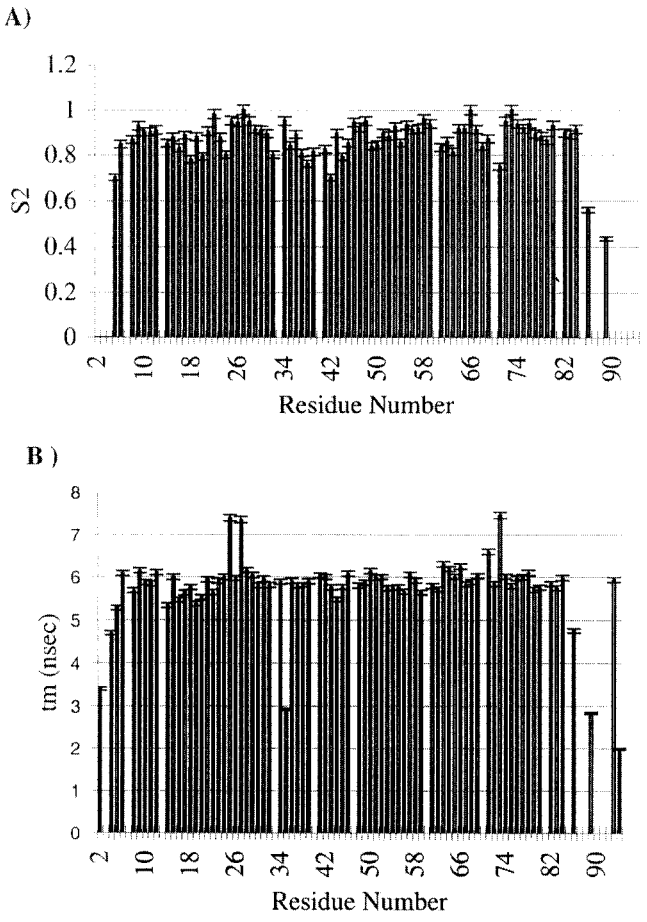

FIGURE 13: (A) A plot of the square of the generalized order parameters (S^2) plotted against the residue number. (B) A plot of the individual τ_m values for each residue as calculated by the R_2R_1 1.1 program

Sligar. The program MIDAS plus, used in the display of the protein structures, was provided by the computer graphics laboratory at the University of California, San Francisco.

SUPPORTING INFORMATION AVAILABLE

Three tables containing complete sequence specific and conformation specific ^{1}H, ^{15}N, and ^{13}C resonance assignments for rat ferrocytochrome b_5 (Table S-1), a complete listing of restraints used in the calculation of the solution structures of A and B conformations of rat cytochrome b_5 in DIANA 2.1 format (Table S-2), and parameters obtained from the model free analysis for each residue (Table S-3). Coordinates for both equilibrium conformations have been deposited in the Brookhaven Protein Data Bank (53 pages). See any current masthead page for ordering information.

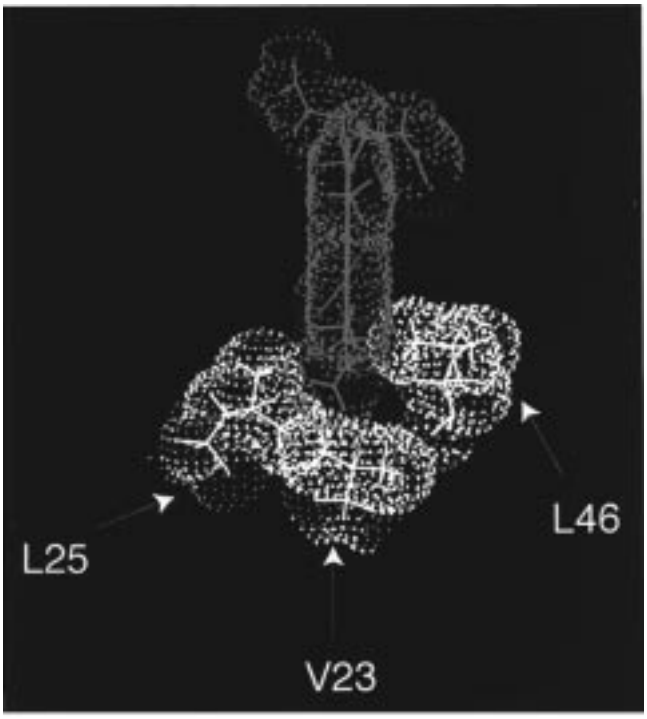

FIGURE 14: A plot showing the van der Waals surface of the heme group, V23, L25, and L46 in the B conformer of the NMR solution structure. The picture shows the interaction of the 2-vinyl group with the hydrophobic residues lining the pocket.

REFERENCES

1. Vergères, G., and Waskell, L. (1995) *Biochemie 77*, 604−620.
2. Rodriguez, M., Qiu, M. J., Stark, R. E., White, S. P., Zhang, X., Foundling, S. I., Rodriguez, V., Schilling, C. L., Bunce, R. A., and Rivera, M. (1996) *Biochemistry 35*, 16378−16390.
3. Mathews, S., Czerwinski, E. W., and Argos, P. (1979) in *The X-ray Crystallographic Structure of Calf Liver Cytochrome b_5* (Mathews, S., Czerwinski, E. W., and Argos, P., Eds.) Vol. VII, pp 107−147, Academic Press, New York.
4. Kelly, G. P., Muskett, F. W., and Whitford, D. (1997) *Eur. J. Biochem. 245*, 349−354.
5. Keller, R. M., and Wüthrich, K. (1980) *Biochim. Biophys. Acta 621*, 204−217.
6. Guiles, R. D., Basus, V. J., Kuntz, I. D., and Waskell, L. (1992) *Biochemistry 31*, 11365−11375.
7. Guiles, R. D., Altman, J., Lipka, J. J., Kuntz, I. D., and Waskell, L. (1990) *Biochemistry 29*, 1276−1289.
8. Guiles, R. D., Basus, V. J., Sarma, S., Malpure, S., Fox, K. M., Kuntz, I. D., and Waskell, L. (1993) *Biochemistry 32*, 8329−8340.
9. Sarma, S., Banville, D., DiGate, R. J., and Guiles, R. D. (1996) *J. Biomol. NMR 8*, 171−183.
10. Muskett, F. W., Kelly, G. P., and Whitford, D. (1996) *J. Mol. Biol. 250*, 172−189.
11. Banci, L., Bertini, I., Ferroni, F., and Rosato, A. (1997) *Eur. J. Biochem. 249*, 270−279.
12. Lee, K. B., La Mar, G. N., Mansfield, K. E., Smith, K. M., Pochapsky, T. C., and Sligar, S. G. (1993) *Biochim. Biophys. Acta 1202*, 189−199.

13. Muskett, F. W., Kelley, G. P., and Whitford, D. (1996) *J. Mol. Biol. 246*, 172−189.
14. Arnesano, F., Banci, L., Bertini, I., and Felli, I. C. (1998) *Biochemistry 37*, 173−184.
15. Salemme, F. R. (1976) *J. Mol. Biol. 102*, 563−568.
16. Wendoloski, J. J., Matthew, J. B., Weber, P. C., and Salemme, F. R. (1987) *Science 238*, 794−797.
17. Mauk, R. M., and Mauk, A. G. (1982) *Biochemistry 21*, 4730−4734.
18. Poulos, T. L., and Mauk, A. G. (1983) *J. Biol. Chem. 258*, 7369−7373.
19. Pochapsky, T. C., Sligar, S. G., McLachlan, S. J., and La Mar, G. N. (1990) *J. Am. Chem. Soc. 112*, 5258−5263.
20. Mortuza, G. B., and Whitford, D. (1997) *FEBS Lett. 412*, 610−614.
21. Storch, E. M., and Daggett, V. (1995) *Biochemistry 34*, 9682−9693.
22. Walker, F. A., Emrick, D., Rivera, J. E., Hanquet, B. J., and Buttlaire, D. H. (1988) *J. Am. Chem. Soc. 110*, 6234−6240.
23. Funk, W. D., Lo, T. P., Mauk, M. R., Brayer, G. D., MacGillivray-Ross, T. A., and Mauk, A. G. (1990) *Biochemistry 29*, 5500−5508.
24. Sarma, S., Banville, D., DiGate, R. J., Miller, C., and Guiles, R. D. (1997) *Biochemistry 36*, 5658−5668.
25. La Mar, G. N., Burns, P. D., Jackson, J. T., Smith, K. M., Langry, K. C., and Strittmatter, P. (1981) *J. Biol. Chem. 256*, 6075−6079.
26. Guiles, R. D., Sarma, S., DiGate, R. J., Banville, D., Basus, V. J., Kuntz, I. D., and Waskell, L. (1996) *Nat. Struct. Biol. 3*, 333−339.
27. Kuboniwa, H., Grzesiek, S., Delaglio, F., and Bax, A. (1994) *J. Biomol. NMR 4*, 871−878.
28. Kay, L. E., Xu, G.-Y., Singer, A. U., Muhandiram, D. R., and Forman-Kay, J. D. (1993) *J. Magn. Reson., Ser. B 101*, 333−337.
29. Grzesiek, S., and Bax, A. (1993) *J. Biomol. NMR 3*, 185−204.
30. Ikura, M., Kay, L. E., and Bax, A. (1990) *Biochemistry 29*, 4659−4667.
31. Mori, S., Abeygunawardana, C., Johnson, M. O. N., and van Zijl, P. C. M. (1995) *J. Magn. Reson., Ser. B 108*, 94−98.
32. Farrow, N. A., Muhandiram, R., Singer, A. U., Pascal, S. M., Kay, C. M., Gish, G., Shoelson, S. E., Pawson, T., Forman-Kay, J. D., and Kay, L. E. (1994) *Biochemistry 33*, 5984−6003.
33. Wishart, D. S., Bigam, C. G., Yao, J., Abildgaard, F., Dyson, H. J., Oldfield, E., Markley, J. L., and Sykes, B. D. (1995) *J. Biomol. NMR 6*, 135−140.
34. Sarma, S., Dangi, B., Yan, C.-H., DiGate, R. J., Banville, D., and Guiles R. D. (1997) *Biochemistry 36*, 5645−5657.
35. Delaglio, F., Grzesiek, S., Vuister, G. W., Zhu, G., Pfeifer, J., and Bax, A. (1995) *J. Biomol. NMR 6*, 277−293.
36. Guntert, P., Werner, B., and Wüthrich, K. (1991) *J. Mol. Biol. 217*, 517−530.
37. Basus, V. J. (1989) *Methods Enyzmol. 177*, 132−149.
38. Laskowski, R. A., MacArthur, M. W., Moss, D. S., and Thornton, J. M. (1993) *J. Appl. Crystallogr. 26*, 477−486.
39. Mandel, A. M., Akke, M., and Palmer, A. G. (1995) *J. Mol. Biol. 246*, 144−163.
40. Grzesiek, S., Bax, A. (1993) *J. Am. Chem. Soc. 115*, 12593−12594.
41. Lipari, G., and Szabo, A. (1982) *J. Am. Chem. Soc. 104*, 4546−4558.
42. Lipari, G., and Szabo, A. (1982) *J. Am. Chem. Soc. 104*, 4559−4570.
43. Abragam, A. (1961) *The Principles of Nuclear Magnetism*, pp 264−349, Clarendon Press, Oxford.
44. Tjandra, N., Feller, S. E., Pastor, R. W., and Bax, A. (1995) *J. Am. Chem. Soc. 117*, 12562−12566.
45. Alam, S. L., Volkman, B. F., Markley, J. L., and Satterlee, J. D. (1998) *J. Biomol. NMR* (in press).
46. Banci, L., Pierattelli, R., and Turner, D. L. (1995) *Eur. J. Biochem. 232*, 522−527.
47. Wishart, D. S., and Sykes, B. D. (1994) *Methods Enzymol. 239*, 363−392.
48. Amburgey, J. C., Abildgaard, F., Starich, M. R., Shah, S., Hilt, D. C., and Weber, D. J. (1995) *J. Biomol. NMR 6*, 171−179.
49. Snedecor, G. W., and Cochran, W. G. (1980) *Statistical Methods*, 7th ed., p 505, The Iowa State University Press.
50. Bruschweiller, R., Liao, X., and Wright, P. E. (1995) *Science 268*, 886−889.
51. Walker, F. A., Huynh, B.-H., Scheidt, W. R., and Osvath, S. R. (1986) *J. Am. Chem. Soc. 108*, 5288−5297.
52. Quinn, R., Mercer − Smith, J., Burstyn, J. N., and Valentine, J. S. (1984) *J. Am. Chem. Soc. 106*, 4136−4144.
53. O'Brien, P., and Sweigart, D. A. (1985) *Inorg. Chem. 24*, 1405−1409.
54. Zhou, H.-X. (1994) *J. Am. Chem. Soc. 116*, 10362−10375.
55. Reid, L. S., Mauk, M. R., and Mauk, A. G. (1984) *J. Am. Chem. Soc. 106*, 2182−2185.
56. Hunter, C. L., Lloyd, E., Eltis, L. D., Rafferty, S. P., Lee, H., Smith, M., and Mauk, A. G. (1997) *Biochemistry 36*, 1010−1017.
57. Hunter, C. L., Mauk, A. G., and Douglas, D. J. (1997) *Biochemistry 36*, 1018−1025.
58. Wishart, D. S., Bigam, C. G., Holm, A., Hodges, R. S., and Sykes, B. D. (1995) *J. Biomol. NMR 5*, 67−81.
59. Wüthrich, (1986) K. *NMR of Proteins and Nucleic Acids*, Wiley-Interscience, New York.
60. Daggett, V., and Levitt, M. (1992) *J. Mol. Biol. 223*, 1121−1138.
61. Swartz, P. D., and Ichiye, T. (1996) *Biochemistry 35*, 13772−13779.
62. Marion, D. (1994) *Biochemie 76*, 631−640.
63. Lyons, T. A., Ratnaswamy, G., and Pochapsky, T. C. (1996) *Protein Sci. 5*, 627−639.
64. Qi, X. P., Beckman, R. A., and Wand, A. J. (1996) *Biochemistry 35*, 12275−12286.
65. Dangi, B., Blankman, J. I., Miller, C. J., Volkman, B. F., and Guiles, R. D. (1998) *J. Phys. Chem., Ser. B* (In press).
66. Durley, R. C., and Mathews, F. S. (1996) *Acta Crystallogr., Sect. D 52*, 65−72.

BI9801964